

UAV remote sensing based estimation of green cover during turfgrass establishment

Tianyi Wang^{a,b}, Ambika Chandra^{b,*}, Jinha Jung^c, Anjin Chang^d

^a College of Engineering, China Agricultural University, P.O. Box 134, No. 17 Qinghua East Road, Haidian District, Beijing 100083, China

^b Texas A&M AgriLife Research, Dallas, TX 75252, USA

^c Lyles School of Civil Engineering, Purdue University, West Lafayette, IN 47907, USA

^d School of Engineering and Computing Science, Texas A&M University-Corpus Christi, Corpus Christi, TX 78412, USA

ARTICLE INFO

Keywords:

Turfgrass
UAV
Remote sensing
Percent green cover
Establishment
Machine learning
Classification

ABSTRACT

Turfgrass is an important urban crop in the United States. Determining the percent green cover (PGC) to assess turfgrass quality/health and the rate of establishment is a crucial parameter for evaluating different species and experimental lines within species. However, evaluating the PGC of individual plots within large breeding nurseries in a conventional way, either visually or through digital image analysis is a time-consuming and laborious process. In the present study, we used the unmanned aerial vehicle (UAV) with multispectral and RGB sensors to estimate PGC during turfgrass establishment. We evaluated thirty approaches with different levels of complexity based on vegetation indices, supervised and unsupervised machine learning classification methods, and image processing methods for high-throughput turfgrass PGC estimation. An HSV (Hue-Saturation-Value) color space-based green pixel identification (GPI) method was introduced for the first time for estimating UAV derived PGC (UAV_{PGC}). The results indicate that the GPI achieved the highest coefficient of determination, 0.86–0.96, with lowest mean absolute error when compared to ground percent green cover (GroundPGC). Overall, UAV-derived RGB image-based support vector machine methods were in agreement with GroundPGC ($R^2 = 0.88–0.95$). This suggests that UAV-derived RGB images are adequate in accurately determining percent green cover (green vegetation within an experimental plot); however, multispectral images might offer a solution to determine turfgrass coverage (green and non-green vegetation within an experimental plot) during turfgrass establishment to account for non-green vegetation which is not captured by RGB (visible light spectrum) based estimation of PGC.

1. Introduction

Turfgrass serves as an important vegetative ground cover worldwide (Emmons and Rossi, 2015) offering many environmental, economic and societal benefits (Brosnan et al., 2020). Percent green cover (PGC), described as a percent of green vegetation per unit area, is a crucial indicator used to evaluate the overall plant health and establishment rate over time. Species and cultivars with faster establishment from plugs or sprigs and higher PGC are favored by turfgrass producers and consumers alike. Conventional visual assessment of turfgrass plots to estimate the amount of green cover, on a percent or 1–9 scale has served as a standard and is routinely used by the turfgrass researchers (Morris and Shearman, 1998). However, collecting visual ratings is a time-consuming and labor-intensive process (Trenholm et al., 1999),

especially for large breeding nurseries, which limits the frequency of data collection. Saturated soil condition after major rainfall event may delay access to the field nurseries and affect timely visual data collection by plant breeders and researchers. Visual assessments are also subjective in nature (Horst et al., 1984) and are inevitably prone to rater's fatigue and rater's bias (personal preference) even if the rater is well-trained. Furthermore, the inconsistency of visual field assessments between different raters as well as optical illusion (Bach and Poloschek, 2006) or the influence of variable weather conditions (cloudiness, shadows, turf wetness) and mowing patterns (direction and height) across different data collection days (Krans and Morris, 2007) can make conducting genetic comparisons difficult.

The quality and frequency of phenotypic data collection at the field scale is currently the bottleneck limiting the efficiency and accuracy of

* Corresponding author.

E-mail address: ambika.chandra@ag.tamu.edu (A. Chandra).

<https://doi.org/10.1016/j.compag.2022.106721>

Received 25 June 2021; Received in revised form 10 January 2022; Accepted 15 January 2022

0168-1699/© 2022 The Authors.

Published by Elsevier B.V. This is an open access article under the CC BY-NC-ND license

(<http://creativecommons.org/licenses/by-nc-nd/4.0/>).

classical phenotype-based plant breeding. Ground-level spectral or proximal sensing methods have been used to address some of the limitations associated with visual field assessments. Proximal digital imagery data has been widely used for pest detection, vegetation management, and green cover estimation (Adamsen et al., 1999). Canopy structure estimation (Tucker et al., 1975), and vegetation indices (VIs) such as the leaf area index (LAI) and green area index (GAI) have been shown to estimate the green cover of shortgrass prairie and provide quantitative vegetation information as compared to qualitative visual ratings (Przeszlowska et al., 2006). Turfgrass researchers routinely use ground-level digital image analysis using the light-box for quantitative estimation of PGC (Richardson et al., 2001). More recently, researchers have been using handheld devices with multispectral sensors to record NDVI (normalized difference vegetation index) on individual plot basis (Bremer et al., 2011). Although collecting such ground-level spectral or proximal data saves resources and offers quantitative assessment, collecting such data frequently on large breeding nurseries is still a time and labor-intensive procedure.

Remote sensing has emerged as an efficient tool to collect quantitative data in a high-throughput manner. It has been widely used in the areas of environment, agriculture and urban planning, (Bégué et al., 2018; de Donato et al., 2016; Huang et al., 2018; Yang et al., 2014). More recently, researchers have shown an increased interest in using unmanned aerial vehicle (UAV) based remote sensing because of its ease of use, ability to acquire fine spatial and high temporal resolution data, as well as lower cost compared to conventional remote sensing platforms (Wang et al., 2020c). Unlike satellite images, UAV data collected on overcast days is generally usable when flight is operated below the cloud level. UAV remote sensing is becoming a popular solution for precision disease delineation, yield estimation, and field management (Ashapure et al., 2020; Bhandari et al., 2020; Chang et al., 2021, 2020, 2017; Duan et al., 2019; Herrmann et al., 2020; Maimaitijiang et al., 2020; Oh et al., 2020; Romero et al., 2018; Su et al., 2018; Wang et al., 2020b, 2020a). UAV remote sensing has been used to monitor the nitrogen status and detect the drought stress in turfgrass systems (Caturegli et al., 2016; Hong et al., 2019b, 2019a). Zhang et al. (2019) have shown the potential utility of UAV-derived vegetation indices (VIs) such as zonal mean normalized difference vegetation index (NDVI) to predict PGC and turfgrass quality. Zonal mean NDVI-based predictions of PGC during turfgrass establishment can potentially be impacted by factors like species, biomass, plant stresses, genetic color, shoot density, and overall plant health. (Campos et al., 2019; Caturegli et al., 2020; Gogoi et al., 2018; Samseemoung et al., 2012). A healthier or denser turfgrass stand could lead to a higher zonal NDVI value and, consequently, higher PGC values as compared to a larger-sized turfgrass stand but with lower color or density ratings. Furthermore, the estimation of NDVI requires the use of multispectral sensors and sophisticated radiometric calibration of these sensors. To generate high-quality indices, the spectral information of each band needs to be converted to reflectance value using either a ground radiometric calibration target or an additional downwelling light sensor, which can lead to an increase in labor and cost

Image processing methods based on visible spectrum (RGB), such as Sigma Scan (Karcher and Richardson, 2005), Image J (Abramoff et al., 2004), Turf analyzer (Karcher and Richardson, 2015) are routinely used to determine PGC in the field. Another algorithm called Canopeo was proposed by Patrignani (2015) to identify green canopy cover based on RGB image with three empirical parameters. Compared to multispectral sensors, the RGB sensors usually offer a cost-effective way to measure canopy cover. Besides, converting RGB images into Hue-Saturation-Value (HSV) color space (Smith, 1978) can help identify a specific color within the visible spectrum. Vegetation can be identified based on HSV color space in the image (Huang et al., 2016; Yang et al., 2015), which has not previously been used to study remote sensing derived turfgrass data.

Classification is a method that can categorize the pixels within an image based on each pixel's spectral features (Kranjcic et al., 2019) and

has been demonstrated to analyze remote sensing data (Fauvel et al., 2008; Gong and Howarth, 1992; Lu and Weng, 2007; Mountrakis et al., 2011; Pal and Mather, 2005). The pixels or objects in the image are classified according to the land cover themes. Support vector machine (SVM), maximum likelihood classification (MLC), minimum distance classification (MDC), k-means, and ISODATA classification have been shown to effectively distinguished spectral information of vegetation from the soil (Yang et al., 2015). Supervised classification methods such as SVM, MLC, and MDC require training data to train the models, and can usually achieve better accuracy than unsupervised classification methods such as k-means and ISODATA (Wang et al., 2020b; Yang et al., 2015). On the other hand, unsupervised classifications offer more automated procedures than supervised classification. We believe that both supervised and unsupervised machine learning classifications based on visible and infrared spectral bands could potentially be introduced to measure percent green cover within a plot during turfgrass establishment.

To overcome the shortcomings of conventional methods used for estimating turfgrass green cover and to benefit from high-resolution RGB and multispectral images, the specific objectives of this study are: (1) introduce and compare different approaches to estimate percent green cover during turfgrass establishment using UAV-derived data; (2) demonstrate the effectiveness of UAV-derived percent green cover estimation by comparing it to ground-level percent green cover data.

2. Materials and methods

2.1. Study site

This study was conducted at Texas A&M AgriLife Research and Extension Center in Dallas, TX (32°59'10.8"N 96°45'49.4"W) (Fig. 1). The soil order is Vertisol and type is Austin silty clay composed of 45% clay, 7% sand, and 48% silt (<http://websoilsurvey.nrcs.usda.gov/>). Single-spaced-plant nurseries (SSPNs) for zoysiagrass (*Zoysia* spp.) and seashore paspalum (*Paspalum vaginatum* Sw.) were planted on July 21, 2020, as part of the USDA-NIFA funded SCRI project # 2019-51181-30472. A total of 225 zoysiagrass and 94 seashore paspalum entries were planted separately using a randomized complete block design with two replications and a single plug (3" x 3") per replication. Immediately after planting, the study site was rolled with a 2268 kg (5000 lb) roller and supplied with 0.022 kg m⁻² (4.5 lb per 1000 ft⁻²) of Andersons [5-0-10 N-P-K fertilizer and Oxadiazon (Ronstar G)] for pre-emergent weed

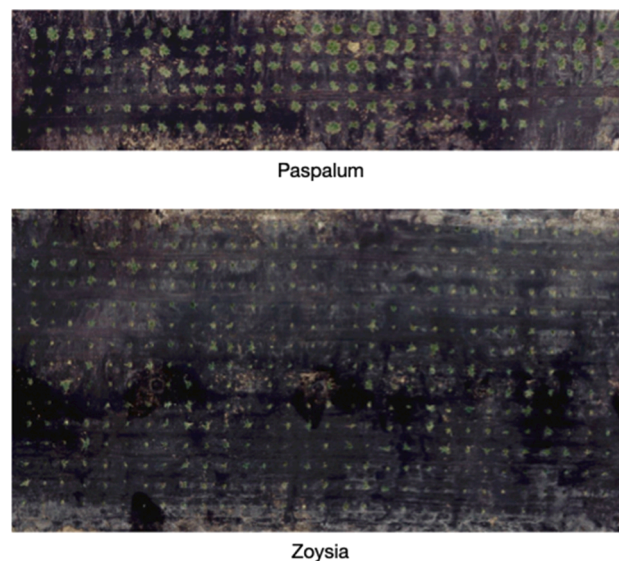


Fig. 1. The study was conducted at a portion of 0.05 km² field in Dallas, TX: 94 seashore paspalum and 225 zoysia grass plots.

control. Additional fertilizer (Harrell’s 42–0–0 N-P-K) was applied in August and September at a rate of 0.005 kg m^{-2} (1 lb N per 1000 ft^{-2}) per month. Weekly mowing was initiated one-month post-planting at 3.81 cm height by using a reel mower, and manual weeding was performed on an as-need basis to maintain plots weed free. Adequate irrigation to supplement rainfall was provided to prevent stress and to promote growth and establishment of plots.

2.2. Data collection

A rotary-wing UAV DJI Matrice 200 V2 (DJI Technology Inc., Shenzhen, China) was used to acquire imagery data on September 24 and October 16, 2020 (Fig. 2a). A multispectral sensor SlantRange 4P+ (SlantRange Inc., San Diego, CA, USA) was mounted on the UAV to collect multispectral images (Fig. 2b). The sensor collected images in six bands which contains three wide visual bands: blue ($470 \pm 55 \text{ nm}$), green ($520 \pm 55 \text{ nm}$), red ($620 \pm 55 \text{ nm}$), and three narrow bands: red ($650 \pm 20 \text{ nm}$), red edge ($715 \pm 15 \text{ nm}$), NIR ($850 \pm 35 \text{ nm}$). The images were collected at 70-m above ground level (AGL), which resulted in orthomosaic images with a spatial resolution of 1.55 cm Ground Sampling Distance (GSD). A 75% forward and side overlap was used for all the UAV data acquisition. The multispectral sensor is equipped with an ambient illumination sensor (AIS) which collects the environmental light condition and converts the at-sensor radiance into absolute surface reflectance value (Ashpуре et al., 2019). Eight ground control points (GCPs) were placed at four corners and four edge midpoints of the fields for geo-referencing. Emlid Reach RS + RTK GNSS receivers (a rover and a base) (Emlid, Hong Kong, China) were used to get precision location coordinates of GCPs.

A commercial RGB camera Canon PowerShot G16 (Canon, Ota City, Tokyo, Japan) was mounted on the top cover of a light-box (Fig. 3) facing the ground and used for ground-level digital image collection (Karcher and Richardson, 2005). The camera was set in auto mode with a graphic ratio of 1:1. The dimension of the box is $0.6 \times 0.5 \times 0.5 \text{ m}$ (L \times W \times H). There are four LED cold light illuminators distributed at the corners inside the box facing the ground for consistent lighting conditions. The ground images of 188 seashore paspalum plots and 440 zoysiagrass plots were collected one by one on September 25 and October 21 (Table 1). Each captured image covered a $0.5 \times 0.5 \text{ m}^2$ ground area.

2.3. Data pre-processing

To make the data comparable, the plots with grass coverage outside the dimension of the light-box were excluded such that a total of 112 seashore paspalum plots (out of 188) and 426 zoysiagrass plots (out of 450) were used for analyzing the first round of collected data. For the second round of data collection, 48 seashore paspalum and 360



Fig. 3. The light-box was used to mount a camera for the collection of ground imagery data.

Table 1

The timeline for data collection of UAV imagery and ground imagery.

	1st round data collection	2nd round data collection
UAV imagery data	September 24, 2020	October 16, 2020
Ground imagery data	September 25, 2020	October 21, 2020

zoysiagrass plots remained inside the dimension of the lightbox and were used for data analysis. The ground-level images were processed using Sigma Scan Pro software (Systat Software Inc, San Jose, CA, USA) to obtain ground PGC referred to as $\text{ground}_{\text{PGC}}$ in this research. We refer to the UAV-derived turfgrass PGC as UAV_{PGC} for differentiation.

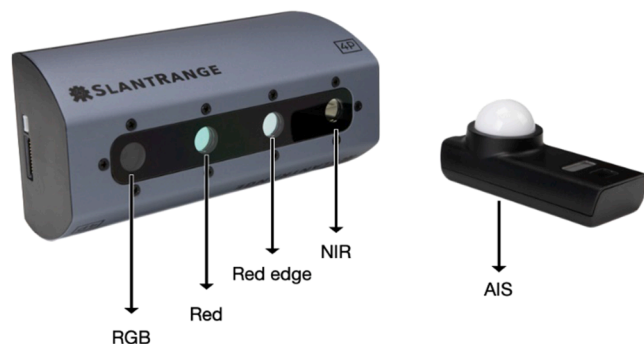
The collected UAV data includes raw imagery, Global Navigation Satellite System (GNSS), and inertial measurement unit (IMU) data. The raw imagery data were pre-processed and calibrated using SlantView (SlantRage, San Diego, CA, USA) software to perform radiometric calibration, and then the radiometrically calibrated images were processed using Pix4D mapper (Pix4D S.A, Lausanne, Switzerland) to generate orthomosaic images.

2.4. UAV-derived turfgrass green cover methods evaluation and comparison

Considering the accuracy, ease of use, and potential cost, a total of thirty turfgrass green cover estimation methods based on UAV data were selected to be evaluated and compared (Table 2). The methods include the combinations of different data processing approaches associated



(a)



(b)

Fig. 2. The images were captured using (a) DJI Matrice 200 V2 UAV platform with a (b) SlantRange 4P + multispectral sensor.

Table 2

Different methods and spectral bands were used to analyze UAV-derived images for determining the percent green cover of turfgrass.

Categories	Methods [†]	6-band composites	CIR composites	RGB composites
2-class unsupervised classification	k-means (2-class)	X	X	X
VIs with unsupervised classification	ISODATA (2-class)	X	X	X
	NDVI based k-means		X	
Image processing	NDRE based k-means		X	
	Green Pixel Canopeo			X
10-class combined unsupervised classification	Canopeo			X
	k-means (10-class combined)	X	X	X
VIs with threshold	ISODATA (10-class combined)	X	X	X
	NDVI with threshold		X	
	NDRE with threshold		X	
	VARI with threshold			X
Supervised classification	SVM	X	X	X
	MLC	X	X	X
	MDC	X	X	X
Mean VIs	Zonal mean NDVI		X	
	Zonal mean NDRE		X	

[†] Thirty different methods used in the current study. Blue color = Low complexity methods; Green color = Moderate complexity methods; Yellow color = High complexity methods.

with the corresponding required imagery data type. The data type includes 6-band multispectral imagery data (blue, green, red-wide, red-narrow, red edge, NIR), 3-band colored-infrared (CIR) composite multispectral imagery data (green, red, NIR), RGB imagery data (red, green, and blue), and VI imagery data. The thirty methods can be summarized into different workflows based on the working principle (Fig. 4) which includes unsupervised and supervised classification, VIs based unsupervised classification, zonal mean VIs, VIs with threshold, and image processing.

We have summarized these thirty methods into three levels of complexities based on the time or steps required to determine turfgrass PGC as well as the need for user's prior knowledge in the area of machine learning. Unsupervised methods such as 2-class k-means or 2-class ISODATA, require fewer number steps or prior knowledge to determine turfgrass plot green cover and therefore, were placed in the low complexity group, whereas unsupervised methods such as green pixel, Canopeo, combined 10-class unsupervised classification, and VIs (NDVI, NDRE, and VARI) with threshold, requires parameter estimation and tuning by a knowledgeable user and were therefore, placed in the moderate level of complexity. Supervised classification methods (SVM, MLC, and MDC) generally require time and an experienced user to train the data set and therefore was placed in the high complexity group. For calculating zonal mean VIs (NDVI and NDRE), the user needs the ground-truth data for conducting the regression analysis and therefore, was also grouped as high complexity level methods.

2.4.1. Machine learning based on multispectral images

With machine learning classification methods, the high-throughput PGC estimation methods can be achieved. The classification based PGC estimation procedure can be summarized into two main steps: (1) The pixels of vegetation were differentiated from the pixels of soil or other non-vegetation objects, and (2) the classification map is used to

derive the PGC. Each pixel in the image was categorized into "grass" or "non-grass" based on spectral information and then formed a binary image. In the present study, "grass" pixel refers to plant tissue with only green leaves. Counting the number of "grass" pixels would lead us to determine the PGC of turfgrass within a plot (Fig. 5). Supervised classification (SVM, MLC, MDC) and unsupervised classification (k-means, ISODATA) algorithms were evaluated for their performance of PGC estimation as different machine learning approaches. Different band composites including 6-band (blue, green, red, red-narrow, red edge, NIR), RGB-band (blue, green, red), and CIR-band (green, red, NIR) were also compared to provide researchers information on the flexibility and practicality of using different types of sensors for estimating turfgrass plot green cover. On each date, the supervised classifications were applied to each band-composite to generate a 2-class classification using the training data. The unsupervised classifications were applied to three different band-composites to generate 2-class and 10-class classifications, respectively. The 10-class unsupervised classification requires an extra step of merging ten classes into 2-classes to generate a binary green cover image.

The polygons of size $0.5 \times 0.5 \text{ m}^2$, the same size as the light-box, were drawn for each plot in QGIS software (Open source). The number of pixels of each class (grass or non-grass) in each plot were counted using QGIS zonal statistics tool and eventually were used for calculating PGC using the following formula:

$$PGC = \frac{\text{Number of grass pixels}}{\text{Number of total pixels}} \quad (1)$$

Where PGC is percent green cover

2.4.2. Mean vegetation indices

The mean NDVI and NDRE values were generated to compare with the classification-derived PGC. The NDVI and NDRE images were calculated in ENVI (Harris geospatial solution, Boulder, CO, USA) by using the Formula (2) and (3) and the mean NDVI and NDRE of each $0.5 \times 0.5 \text{ m}^2$ plots were calculated using QGIS zonal statistics tool.

$$NDVI = \frac{(NIR - red)}{(NIR + red)} \quad (2)$$

$$NDRE = \frac{(NIR - rededge)}{(NIR + rededge)} \quad (3)$$

Where *NIR* is the reflectance of near-infrared band at 850 nm; *Red* is the reflectance of the narrow red band at 650 nm; *Red edge* is the reflectance of the red edge band at 715 nm.

2.4.3. Vegetation indices with thresholds

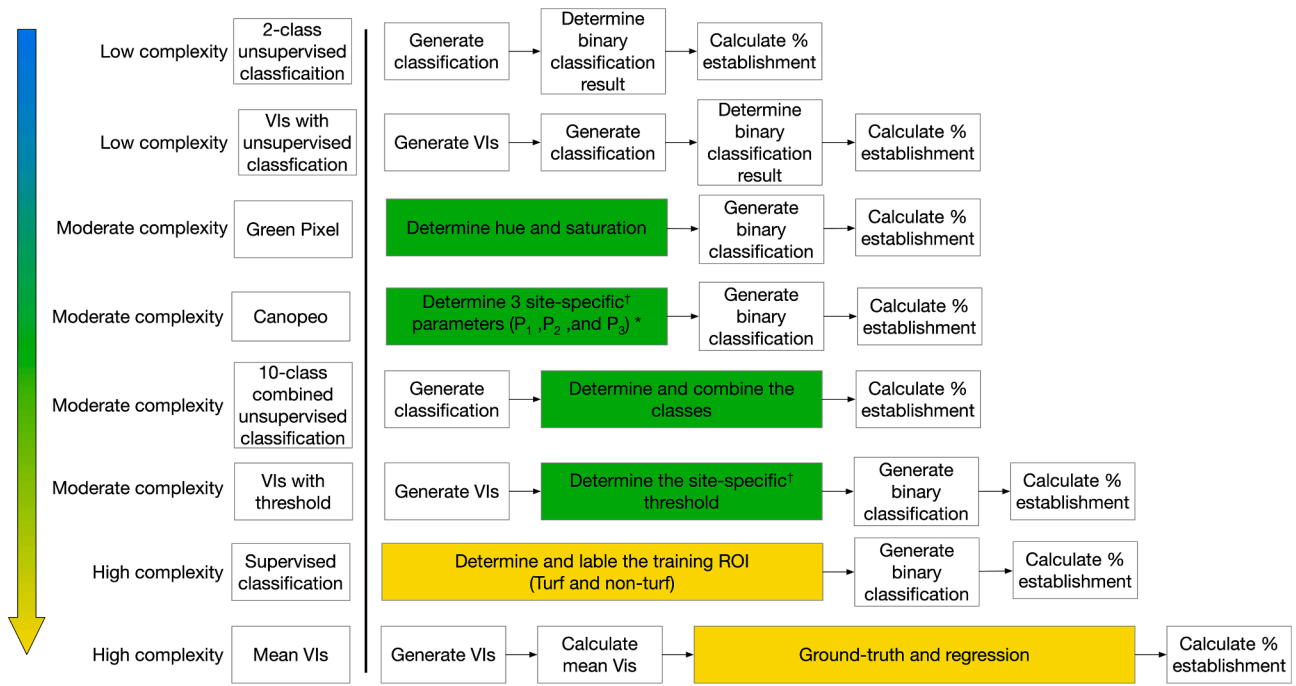
Mean VIs could indicate the overall growth status in the plot, but it cannot indicate the percentile value of green cover directly. Instead, an empirical threshold can be determined to covert the VI image into a binary image. In our case, the threshold value of 0.3 and 0.2 were empirically determined for NDVI and NDRE, respectively. In each $0.5 \times 0.5 \text{ m}^2$ plot, the pixels with a value larger than the thresholds were regarded as established regions and used to calculate the percent plot cover. The Visible Atmospherically Resistant Index (VARI) (Formula 4), as a popular vegetation index using a visible range of the spectrum, was also evaluated with a threshold of 0.

$$VARI = \frac{(green - red)}{(green + red - blue)} \quad (4)$$

Where *blue* is the reflectance at 470 nm; *green* is the reflectance at 520 nm; *Red* is the reflectance at 620 nm.

2.4.4. Machine learning based on vegetation indices

The empirical threshold values are usually determined based on the characters of sensors, light condition, soil types, and species, and so forth, which are not likely to be the same from one to another, or one



Note: † Site refers soil, turfgrass species, sensors and factors may vary by cases

* $P_1, P_2,$ and P_3 are three empirical parameters of Canopeo algorithm

Fig. 4. Nine different workflows of studied methods in the order from low to high complexity. The green box represents procedures required empirical parameters tuning or determining. The yellow box represents procedures of algorithm training or ground-truth data regression. (For interpretation of the references to color in this figure legend, the reader is referred to the web version of this article.)

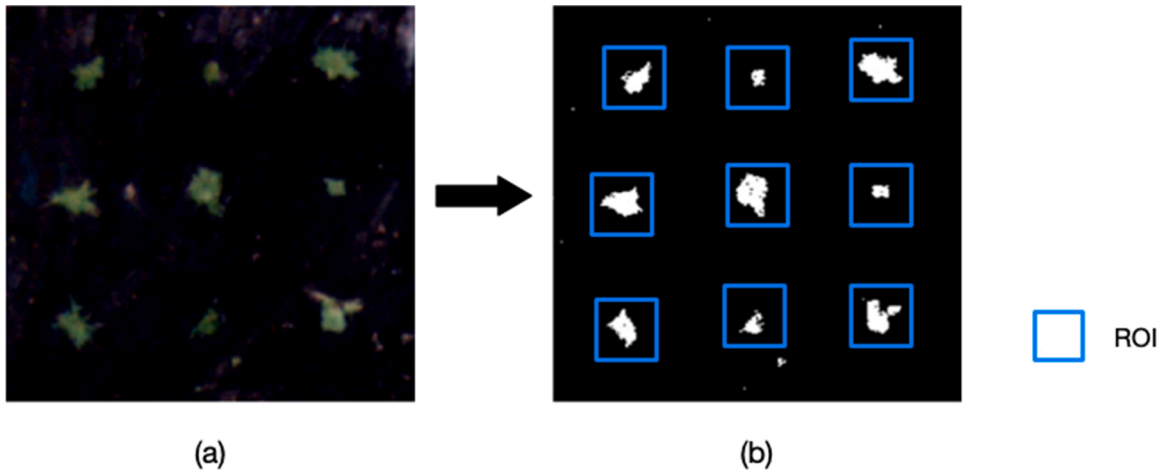


Fig. 5. (a) Nine seashore paspalum plots shown in RGB composites were classified into (b) binary classification. The pixels of the grass class are shown in white while the pixels of the non-grass class are shown in black. The PGC of each plot was calculated within each corresponding ROI. The ROI is in size of $0.5 \times 0.5 \text{ m}^2$ which is the same as the ground and UAV data processing area.

location to another. In other words, expertise and labor are also required for the empirical thresholding VIs approaches. Unlike thresholding VI approaches, applying 2-class k-means classification to VI images with adequate iteration can generate binary maps automatically without any empirical parameters. NDVI and NDRE images were used in this study to demonstrate the 2-class k-means classification to calculate PGC.

2.4.5. RGB image processing approaches

Canopeo, an algorithm that can measure the green canopy cover, was also tested and evaluated in this study. The green cover was identified if

the following criteria were met:

$$\frac{Red}{Green} < P_1 \text{ and } \frac{Red}{Green} < P_2 \text{ and } 2 \times Green - red - blue > P_3 \quad (5)$$

Where *blue* is the reflectance of the blue band at 470 nm; *green* is the reflectance of the green band at 520 nm; *Red* is the reflectance of the narrow red band at 620 nm. In this study, $P_1 = 1.2$, $P_2 = 1.2$, and $P_3 = 2$

In addition to the Canopeo algorithm, we also introduced a new turfgrass PGC estimation approach for turfgrass that is based on HSV color space called Green Pixel Identification (GPI). The RGB image was

first converted to HSV color space so that all pixels in the image could be represented using hue, saturation, and value. The hue value represents all of the visible colors in 360°. The saturation represents the intensity and brilliance of the color on a scale of 0–100, while the value represents the brightness of the color on a scale of 0–100. The median hue value of green color is approx. 120. A minimum of saturation should be set to avoid wrongly identifying the bright colored soil. A minimum value could also be set to avoid misclassifying dark pixels. The hue, saturation, and value are adjustable to fit different turfgrass species and sensors. The algorithm was developed using Python (Python Software Foundation, Wilmington, DE, USA) and is available to researcher by contacting the corresponding author. In this study, green pixels were identified using a tolerance of 20 hue and a minimum saturation of 20 as criteria (Fig. 6):

$$100 < Hue < 140 \text{ and } 20 < Saturation < 100 \quad (6)$$

Where Hue is on a scale of 0–360; Saturation is on a scale of 0–100

2.5. Error assessment

A robust estimation method not only needs a high coefficient of determination but also requires low errors in predictions. Besides coefficient of determination, we used mean absolute error (MAE) as another important criterion to evaluate the methods. MAE is the average of the difference between predicted and actual values. The smaller the MAE, the more accurate the prediction method. The MAE values were calculated using SPSS (IBM, New York, NY, USA).

$$MAE = \frac{\sum_{i=1}^n |y_i - x_i|}{n} \quad (7)$$

Where MAE is mean absolute error; y_i is the predicted value; x_i is the true value; n is the total number of data points.

3. Results and discussion

3.1. Overall comparison between methods

The coefficient of determination between $Ground_{PGC}$ and UAV_{PGC} using thirty approaches was determined for both seashore paspalum

(Fig. 7) and zoysiagrass (Fig. 8). Results showed that 19 out of 30 methods tested for seashore paspalum have the average coefficient of determination (R^2) larger than 0.80 (Fig. 7, Table 3). The GPI with the highest correlation of 0.95 is recognized as a moderate-complexity method, followed by another moderate-complexity method, NDVI-threshold (0.93). The top 10 methods group either in moderate or high complexity level. The low-complexity method that has the highest correlation with ground data is NDVI_k-means (0.90), ranking #11 among the comparison.

Likewise for zoysiagrass, 13 out of 30 methods tested show an average coefficient of determination (R^2) larger than 0.80 (Fig. 8, Table 3). The RGB_SVM, categorized as a high-complexity method, achieved the highest correlation followed by GPI categorized as a moderate-complexity method. The low-complexity method with the highest correlation with ground data is NDVI_k-means (0.85), ranking #8 among the comparison.

In this study, a laptop with Intel i7 9750H CPU associated with 32 GB RAM was used for the data analysis. As low complexity methods, NDVI_k-means, NDRE_k-means, and all other 2-class unsupervised classification generated the classification result in 3–5 s. Likewise, Green pixel, Canopeo, NDVI threshold, NDRE threshold, and VARI threshold with known parameters achieved this same processing speed. However, determining a proper set of parameters for these methods is basically a process of ‘trial and error’ and generally takes 1–5 min depending on the amount of parameter tuning required. For example, VIs with threshold requires only one parameter tuning (ranging between 0.2 and 0.4) and may take shorter time than Green pixel and Canopeo methods. In our study, Green pixel required two parameters which are also located within certain range; whereas, Canopeo required three ratio parameters. For 10-class classification, combining classes into 2-class classification may take approximately 5 min for each run. For supervised classification, selecting and training data with 10 ROIs for two classes generally took 5–10 min. Besides, selecting proper ROIs requires certain level of expertise. The description provides the rationale behind categorizing these methods into low, moderate, and high complexity.

Although the absolute R^2 value of the methods showed a difference, the relative performance of methods showed an agreement between the two species, especially for the top-ranked methods. The methods with the highest seven R^2 value of seashore paspalum are the same as

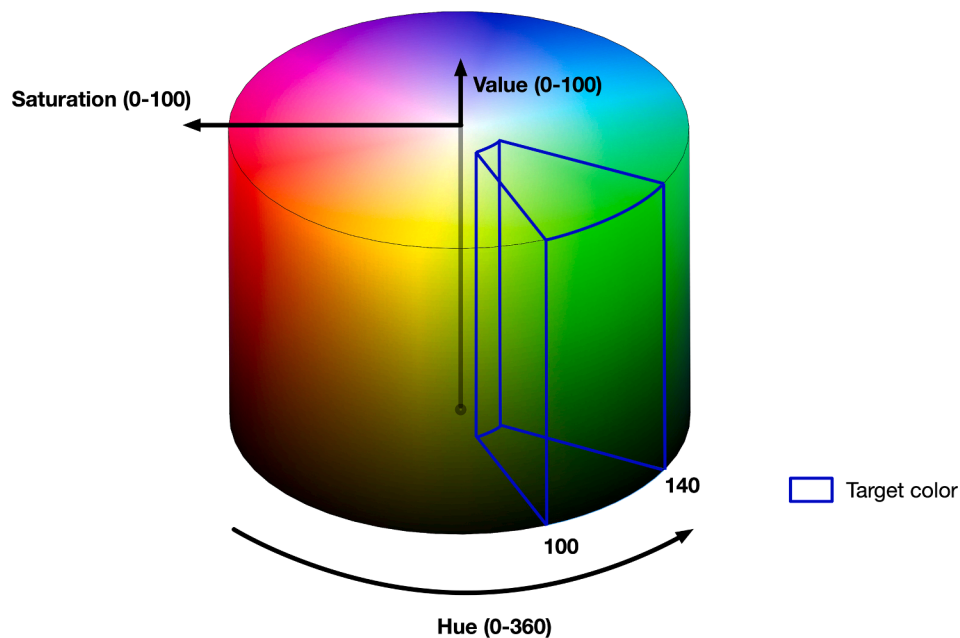


Fig. 6. Green color with the hue of 100–140 and saturation of 20–10 was identified from the image mosaics. (For interpretation of the references to color in this figure legend, the reader is referred to the web version of this article.)

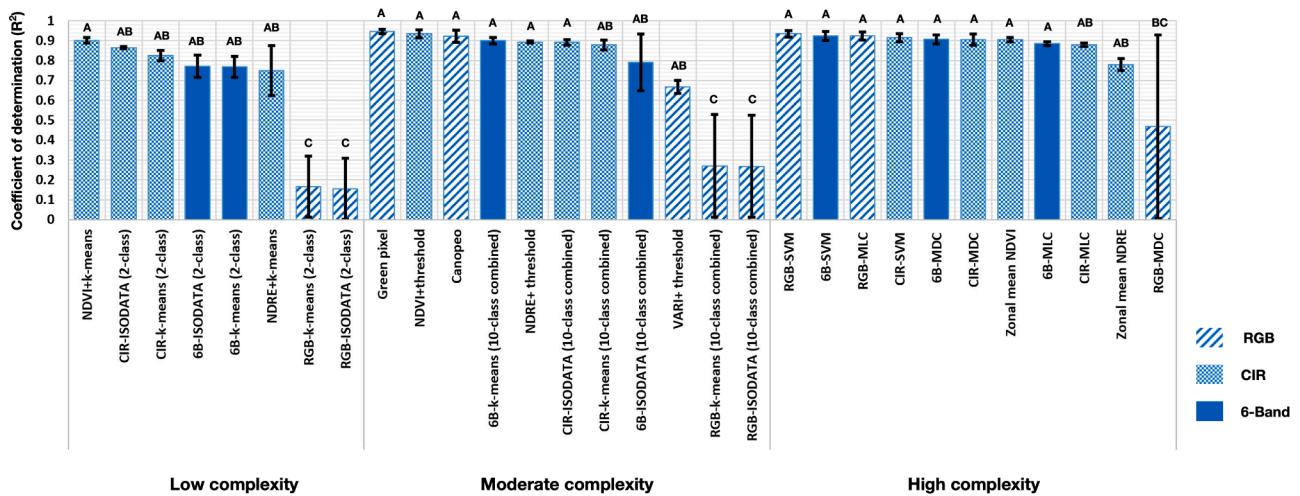


Fig. 7. The coefficient of determination comparison of seashore paspalum between UAV_{PGC} and Ground_{PGC} using different methods. UAV data were collected on September 24 and October 16, and ground data were collected on September 25 and October 21 in 2020. Letter A, B, and C above bars indicate different statistical groups ($\alpha = 0.05$, Duncan test).

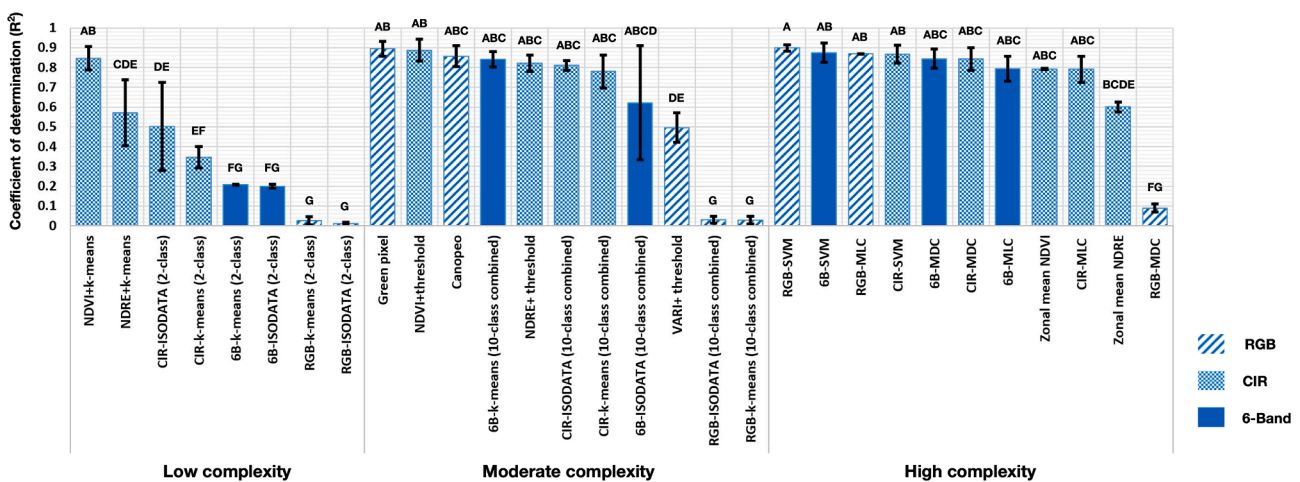


Fig. 8. The coefficient of determination comparison of Zoysiagrass between UAV_{PGC} and Ground_{PGC} using different methods. UAV data were collected on September 24 and October 16, and ground data were collected on September 25 and October 21 in 2020. Letter A, B, and C above bars indicate different statistical groups ($\alpha = 0.05$, Duncan test).

zoysiagrass, referenced as the top 7 methods in the later section. Among the top 7 methods, GPI, NDVI_{threshold}, and Canopeo are moderate-complexity methods, while RGB_{SVM}, 6B_{SVM}, RGB_{MLC}, and CIR_{SVM} are high-complexity methods. NDVI_{k-means} has the highest R² value among all low-complexity methods.

Compared to seashore paspalum, the R² value of zoysiagrass is relatively lower. By Oct.16, 2020, the seashore paspalum had an average ground_{PGC} of 23.08 %, while zoysiagrass only had ground_{PGC} of 11.13 %. Similar results were found by Zhang et al. (2019) where the zoysiagrass has a relatively lower PGC than bermudagrass (*Cynodon* spp.). The slower growth rate and consequently, smaller plot coverage of zoysiagrass at the time of data collection may have potentially led to a lower correlation. First, misclassification was commonly observed at the boundary of the object, known as the boundary effect (Wang et al., 2020b). A smaller patch of grass may lead to a higher percent of boundary pixels. Additionally, non-green vegetation due to injury to pesticide application, or environmental stress or new stolon growth on the edges which may appear as non-green pixels in RGB imagery but still exhibit strong reflectance in the NIR spectrum because of the presence of chlorophyll in the plant tissue (Fig. 9). This helps explain why some RGB-based UAV_{PGC} approaches, such as GPI and RGB_{SVM}, demonstrated

better relationship with RGB-based Ground_{PGC} as compared to the multispectral imagery. These results also suggest that RGB based methods are suitable for estimating percent green cover but multi-spectral imagery may be more suitable in estimating turfgrass coverage which would include green and non-green “grass” pixels (Figs. 9 & 10).

3.2. Error assessment

Mean absolute error (MAE) shows an overall agreement to the coefficient of determination, but it can also indicate the shift of prediction results. For example, NDVI_{k-means} has an R² ranging from 0.92 to 0.89 for paspalum, but it overestimated 12.7 to 13.9% absolute PGC in this case. The methods with the MAE lower than 5 % for seashore paspalum are GPI (2.4%), RGB_{SVM} (3.0%), NDVI_{threshold} (4.1%), 6B_{SVM} (4.6%), Canopeo (4.7%), 6B_{MDC} (4.9%), CIR_{SVM} (4.9%), and CIR_{MDC} (4.9%) (Fig. 11, Table 4). Mean NDVI and Mean NDRE cannot be evaluated because they were not in percentile format.

The methods with the MAE lower than 5 % for zoysiagrass are GPI (2.1%), RGB_{SVM} (2.4%), 6B_{SVM} (2.7%), CIR_{SVM} (2.8%), CIR_{MDC} (2.8%), 6B_{MDC} (2.9%), 6B_{10-class combined k-means} (3.0%), Canopeo (3.2%), RGB_{MLC} (3.3%), 6B_{10-class combined ISODATA} (3.3%),

Table 3
The coefficient of determination between tested methods and ground truth data of 1st and 2nd round data collection.

		Seashore paspalum					Zoysiagrass					
		1st round	2nd round	Average	St. Dev.	S.E.	1st round	2nd round	Average	St. Dev.	S.E.	
Low complexity	NDVI_k-means	0.9158	0.8874	0.9016	0.0201	0.0142	0.9063	0.7868	0.8465	0.0845	0.0598	
	CIR_ISODATA (2-class)	0.8593	0.8705	0.8649	0.0079	0.0056	0.2788	0.7242	0.5015	0.3150	0.2227	
	CIR_k-means (2-class)	0.8519	0.7992	0.8256	0.0373	0.0263	0.2927	0.4007	0.3467	0.0764	0.0540	
	6B_ISODATA (2-class)	0.8263	0.7157	0.7710	0.0782	0.0553	0.1901	0.2098	0.1999	0.0139	0.0098	
	6B_k-means (2-class)	0.8208	0.7157	0.7683	0.0743	0.0526	0.2061	0.2098	0.2079	0.0026	0.0018	
	NDRE_k-means	0.6241	0.8742	0.7492	0.1769	0.1251	0.4045	0.7379	0.5712	0.2357	0.1667	
	RGB_k-means (2-class)	0.3204	0.0117	0.1660	0.2183	0.1543	0.0042	0.0458	0.0250	0.0294	0.0208	
	RGB_ISODATA (2-class)	0.3091	0.0014	0.1553	0.2176	0.1538	0.0034	0.0166	0.0100	0.0094	0.0066	
	Moderate complexity	Green pixel	0.9565	0.9351	0.9458	0.0151	0.0107	0.9332	0.8575	0.8953	0.0535	0.0378
		NDVI_threshold	0.9545	0.9139	0.9342	0.0287	0.0203	0.9428	0.8317	0.8873	0.0786	0.0555
Canopeo		0.9526	0.8930	0.9228	0.0421	0.0298	0.9101	0.8046	0.8574	0.0746	0.0528	
6B_k-means (10-class combined)		0.9158	0.8836	0.8997	0.0228	0.0161	0.8798	0.8028	0.8413	0.0545	0.0385	
NDRE_threshold		0.8987	0.8874	0.8930	0.0080	0.0057	0.8630	0.7815	0.8222	0.0577	0.0408	
CIR_ISODATA (10-class combined)		0.9044	0.8780	0.8912	0.0187	0.0132	0.8354	0.7850	0.8102	0.0356	0.0252	
CIR_k-means (10-class combined)		0.9025	0.8538	0.8781	0.0345	0.0244	0.8630	0.6972	0.7801	0.1172	0.0829	
6B_ISODATA (10-class combined)		0.9332	0.6480	0.7906	0.2016	0.1426	0.9101	0.3329	0.6215	0.4081	0.2886	
VARI_threshold		0.6352	0.6989	0.6671	0.0450	0.0318	0.4225	0.5700	0.4963	0.1043	0.0738	
RGB_k-means (10-class combined)		0.5285	0.0117	0.2701	0.3655	0.2584	0.0079	0.0467	0.0273	0.0274	0.0194	
High complexity	RGB_ISODATA (10-class combined)	0.5242	0.0117	0.2679	0.3624	0.2563	0.0132	0.0467	0.0299	0.0236	0.0167	
	RGB_SVM	0.9506	0.9178	0.9342	0.0232	0.0164	0.9158	0.8817	0.8988	0.0241	0.0171	
	6B_SVM	0.9467	0.9006	0.9237	0.0326	0.0231	0.9235	0.8263	0.8749	0.0688	0.0486	
	RGB_MLC	0.9448	0.9025	0.9236	0.0299	0.0211	0.8705	0.8668	0.8686	0.0026	0.0019	
	CIR_SVM	0.9351	0.8949	0.9150	0.0284	0.0201	0.9120	0.8226	0.8673	0.0632	0.0447	
	6B_MDC	0.9293	0.8836	0.9064	0.0323	0.0228	0.8930	0.7957	0.8443	0.0688	0.0487	
	CIR_MDC	0.9332	0.8780	0.9056	0.0390	0.0276	0.9006	0.7850	0.8428	0.0817	0.0578	
	Zonal mean NDVI	0.9158	0.8949	0.9054	0.0148	0.0105	0.7957	0.7885	0.7921	0.0050	0.0036	
	6B_MLC	0.8949	0.8742	0.8846	0.0146	0.0103	0.8575	0.7310	0.7943	0.0894	0.0632	
	CIR_MLC	0.8874	0.8705	0.8789	0.0119	0.0084	0.8575	0.7242	0.7908	0.0942	0.0666	
Zonal mean NDRE	0.7500	0.8100	0.7800	0.0425	0.0300	0.5761	0.6257	0.6009	0.0351	0.0248		
RGB_MDC	0.9293	0.0067	0.4680	0.6524	0.4613	0.1102	0.0686	0.0894	0.0294	0.0208		

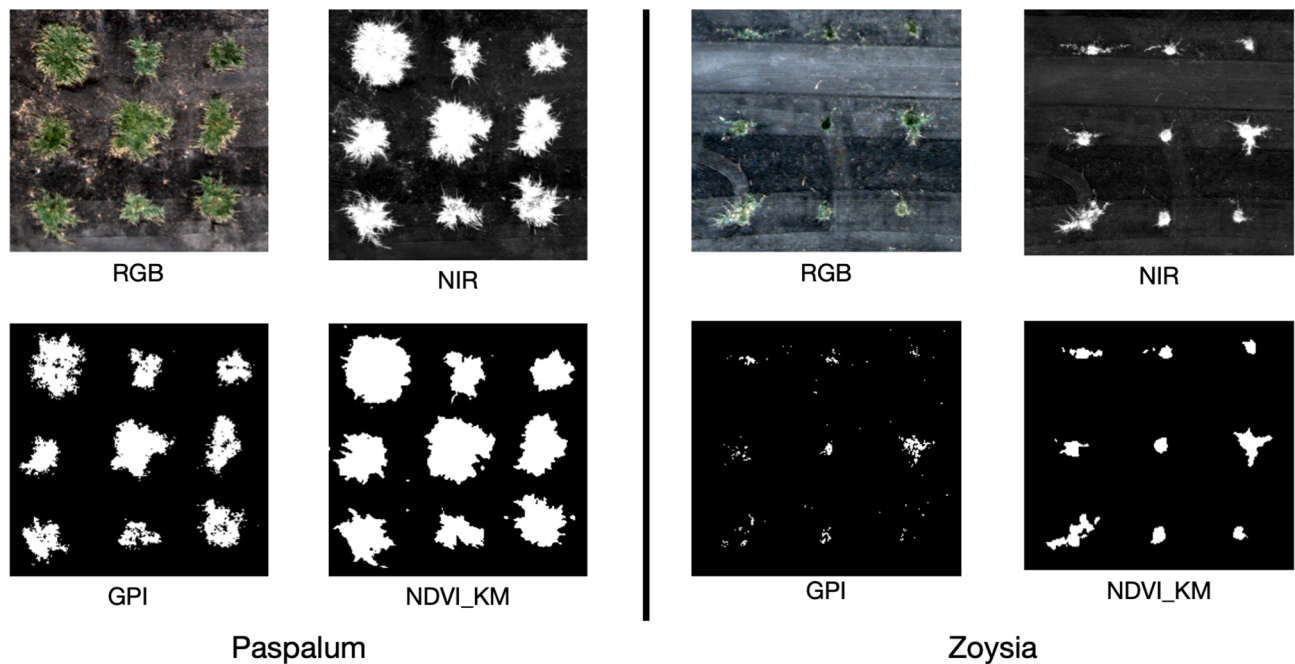


Fig. 9. Stolon around the edges of the plots are visible in RGB composites image but hard to be distinguished in NIR band. The RGB image-based GPI approach shows superior performance in differentiating green grass from dead/dormant grass than the NIR-based methods. (For interpretation of the references to color in this figure legend, the reader is referred to the web version of this article.)

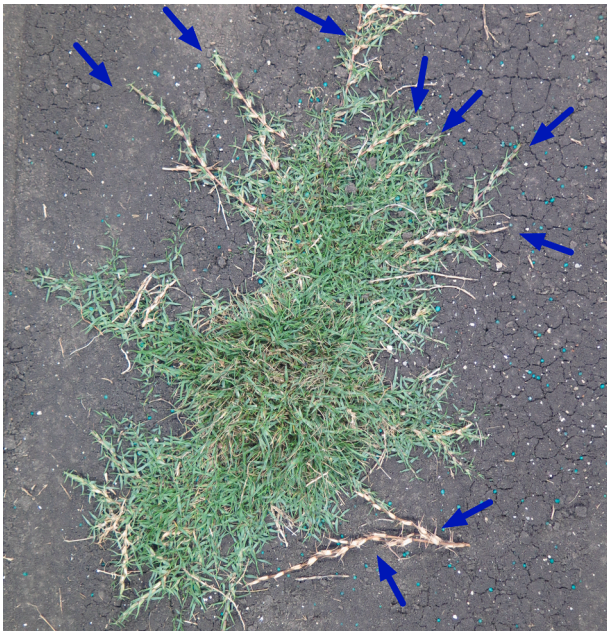


Fig. 10. New stolons (above-ground stems) with young leaves (marked with blue arrows) were classified as “non-grass” (non-green) pixels using RGB-based approaches while multispectral-based methods classified them as “grass” pixels. (For interpretation of the references to color in this figure legend, the reader is referred to the web version of this article.)

CIR_10-class combined ISODATA (3.5%), NDRE_threshold (3.5%), NDVI_threshold (3.6%), CIR_10-class combined k-means (4.7%), and NDVI_k-means (4.8%) (Fig. 12, Table 4).

From the MAE standpoint, the GPI and RGB_SVM methods exhibited the lowest error. The top 7 UAV_{PGC} methods selected based on their high correlation with the ground_{PGC} also ranked in the top 7 methods selected using MAE.

3.3. Zonal mean vegetation index

Zonal mean NDVI achieved 0.91 R² for seashore paspalum and 0.80 for zoysiagrass, while zonal NDRE only achieved 0.78 and 0.60 for seashore paspalum and zoysiagrass, which indicated that zonal mean VIs are useful in estimating turfgrass green cover. In Zhang et al.’s study (2019), the mean NDVI approach achieved a similar result for zoysiagrass (R² = 0.73). However, to obtain the absolute PGC of plots, the

light-box imagery derived ground truth green cover data must be collected each time to establish the mapping rule. Thus, zonal mean VIs are categorized as high-complexity methods. Besides, the detailed distribution information of the turfgrass plots cannot be revealed by mean VIs approaches.

3.4. Classifications based on imagery data

Vegetation indices usually use a limited number of spectral bands. For instance, NDVI is derived using only red and NIR bands, while NDRE only uses spectral information of red edge and NIR bands. However, the six-band composites-based machine learning classifications methods use all available spectral bands’ information, which theoretically should provide more accurate results.

In this study, eight out of nine tested supervised classification exhibited a good correlation between UAV_{PGC} and ground_{PGC} (R² = 0.72–0.95). The result shows that classifications based on three-band CIR composites are as robust as those based on six-band composites, indicating that the information obtained from CIR composites is sufficient to distinguish turfgrass green cover from the soil. On the contrary, RGB composites did not provide adequate information for the minimum distance supervised classification. For example, RGB composites-based MDC could not accurately differentiate between dark color soil and turfgrass with dark greenness and classified them into turfgrass class. The RGB_MDC also mistakenly classified light color soil and turfgrass with light greenness into non-turfgrass class.

The unsupervised classification did not perform as good as supervised classification, especially for the approaches based on RGB composites (R² = 0.00–0.53). Apparently, the clustering algorithm does not distinguish soil and grass accurately using the spectral information from visible bands only. The combined 10-class unsupervised classification with R² value as high as 0.93 had superior performance than 2-class unsupervised classification. However, the performance may not be consistent due to the nature of the clustering principle. The rules of k-means/ISODATA classification were generated based on the separability of all the data points within the region of interest (ROI), which may vary from time to time. For example, the 6B 10-class combined ISODATA achieved R² of 0.93 for the first round of seashore paspalum data but has the R² reduced to 0.65 for the second round of seashore paspalum data. On the contrary, supervised classification, especially SVM, provided an accurate and consistent performance.

In general, the supervised classification has better performance than the unsupervised classification on estimating turfgrass green cover, but the supervised classification requires training data preparation and algorithm training, which are not required in unsupervised classification

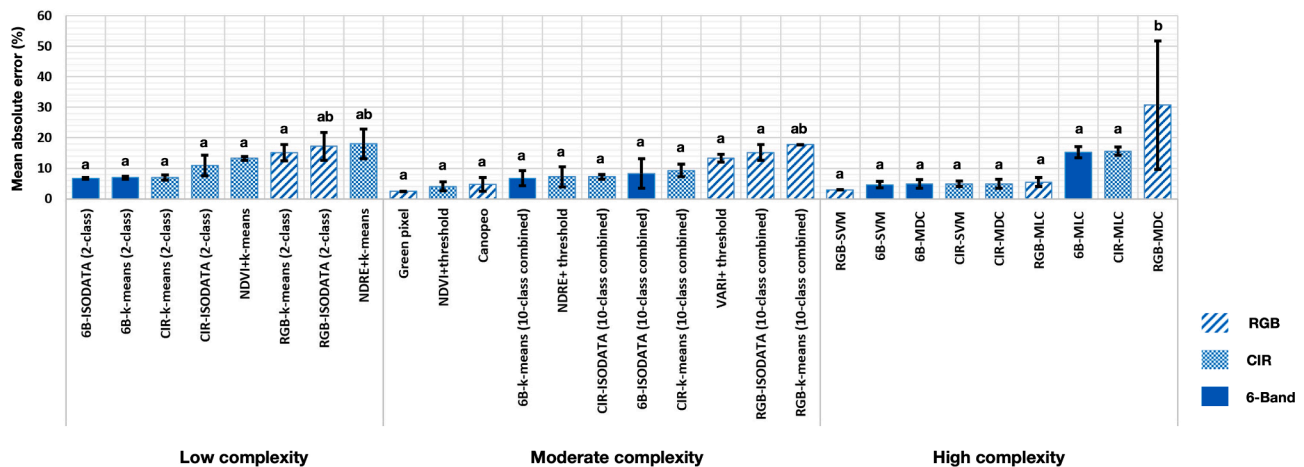


Fig. 11. Mean absolute error comparison of seashore paspalum using UAV_{PGC} versus Ground_{PGC}. UAV data were collected on September 24 and October 16, and ground data were collected on September 25 and October 21 in 2020. Letter a, b, and c above bars indicate different statistical groups ($\alpha = 0.05$, Duncan test).

Table 4
The mean absolute error between tested methods and ground truth data of 1st and 2nd round data collection.

		Paspalum					Zoysia				
		1st round	2nd round	Average	St.Dev.	S.E.	1st round	2nd round	Average	St.Dev.	S.E.
Low complexity	NDVI_k-means	13.9369	12.6727	13.3048	0.8939	0.6321	4.4146	5.1940	4.8043	0.5511	0.3897
	CIR_ISODATA (2-class)	7.6011	14.3449	10.9730	4.7686	3.3719	6.4533	7.9094	7.1813	1.0297	0.7281
	CIR_k-means (2-class)	7.7984	6.0698	6.9341	1.2223	0.8643	6.3306	6.5366	6.4336	0.1457	0.1030
	6B_ISODATA (2-class)	7.0345	6.4270	6.7308	0.4296	0.3038	7.0103	8.1752	7.5927	0.8237	0.5824
	6B_k-means (2-class)	7.4180	6.4270	6.9225	0.7007	0.4955	6.8876	8.1752	7.5314	0.9105	0.6438
	NDRE_k-means	22.9404	13.2111	18.0757	6.8797	4.8647	18.9742	7.0729	13.0236	8.4156	5.9507
	RGB_k-means (2-class)	12.5212	17.8721	15.1966	3.7837	2.6755	11.2637	29.5664	20.4151	12.9419	9.1513
Moderate complexity	RGB_ISODATA (2-class)	12.6284	21.7517	17.1901	6.4511	4.5616	11.3589	13.4733	12.4161	1.4951	1.0572
	Green pixel	2.3825	2.4996	2.4411	0.0828	0.0586	1.8152	2.4592	2.1372	0.4554	0.3220
	NDVI_threshold	2.5890	5.6002	4.0946	2.1292	1.5056	2.1470	5.0602	3.6036	2.0599	1.4566
	Canopeo	2.5253	6.9702	4.7477	3.1430	2.2225	2.0374	4.3159	3.1767	1.6112	1.1393
	6B_k-means (10-class combined)	9.1822	4.2503	6.7162	3.4874	2.4659	3.2976	2.6086	2.9531	0.4871	0.3445
	NDRE_threshold	10.5363	3.8648	7.2006	4.7174	3.3357	4.6640	2.3393	3.5017	1.6438	1.1624
	CIR_ISODATA (10-class combined)	7.9978	6.4625	7.2302	1.0856	0.7677	3.1325	3.8440	3.4882	0.5031	0.3557
	CIR_k-means (10-class combined)	11.3161	7.2222	9.2692	2.8949	2.0470	4.6229	4.6997	4.6613	0.0543	0.0384
	6B_ISODATA (10-class combined)	3.4015	13.1728	8.2871	6.9093	4.8856	1.7967	4.7853	3.2910	2.1132	1.4943
	VARI_threshold	11.9981	14.6001	13.2991	1.8399	1.3010	7.5357	8.2290	7.8823	0.4902	0.3466
High complexity	RGB_k-means (10-class combined)	17.7943	17.8685	17.8314	0.0525	0.0371	28.0091	29.6006	28.8049	1.1254	0.7958
	RGB_ISODATA (10-class combined)	12.5478	17.8685	15.2082	3.7623	2.6603	19.2619	29.6006	24.4313	7.3106	5.1694
	RGB_SVM	2.9602	2.9771	2.9687	0.0120	0.0085	1.9389	2.8468	2.3929	0.6420	0.4539
	6B_SVM	3.5493	5.6878	4.6186	1.5122	1.0693	1.5517	3.9062	2.7290	1.6649	1.1773
	RGB_MLC	7.0191	3.9783	5.4987	2.1502	1.5204	4.0986	2.4165	3.2576	1.1895	0.8411
	CIR_SVM	4.0637	5.7904	4.9270	1.2209	0.8633	1.5656	3.9645	2.7651	1.6963	1.1995
	6B_MDC	3.5181	6.2477	4.8829	1.9302	1.3648	1.9182	3.8163	2.8673	1.3422	0.9490
	CIR_MDC	3.4126	6.4625	4.9375	2.1566	1.5250	1.8524	3.8440	2.8482	1.4082	0.9958
	Zonal mean NDVI	N/A	N/A	N/A	N/A	N/A	N/A	N/A	N/A	N/A	N/A
	6B_MLC	17.0579	13.5012	15.2796	2.5150	1.7784	7.7095	7.0804	7.3950	0.4449	0.3146
CIR_MLC	16.9244	14.3449	15.6347	1.8240	1.2898	7.5812	7.9094	7.7453	0.2321	0.1641	
Zonal mean NDRE	N/A	N/A	N/A	N/A	N/A	N/A	N/A	N/A	N/A	N/A	
RGB_MDC	9.6920	51.7748	30.7334	29.7571	21.0414	6.3772	26.1816	16.2794	14.0038	9.9022	

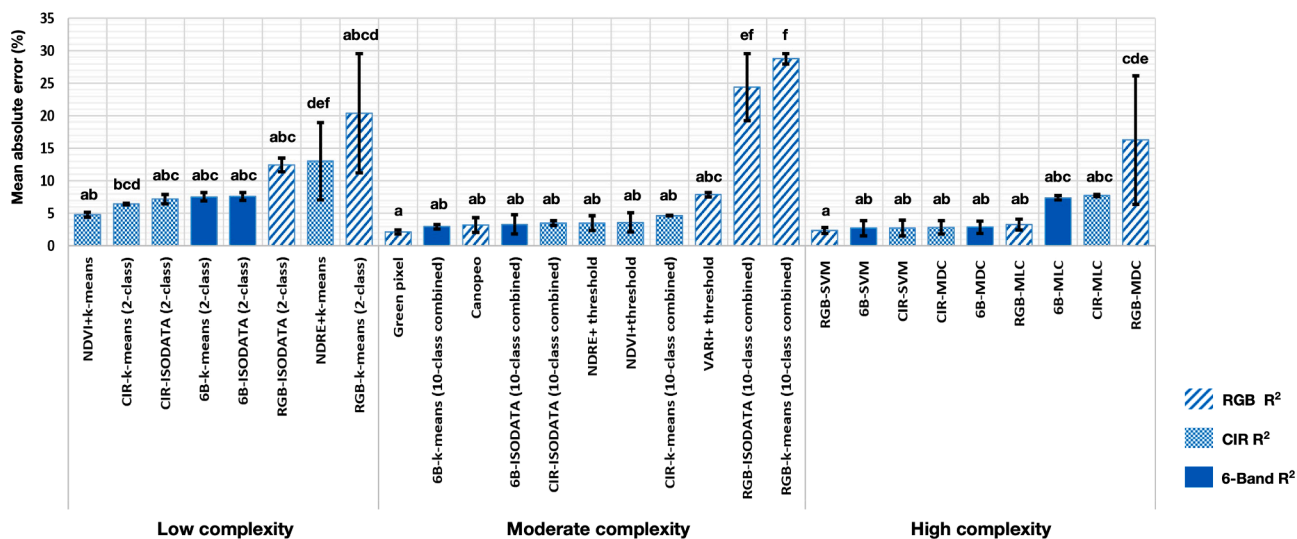


Fig. 12. Mean absolute error comparison of Zoysia using UAV_{PGC} versus Ground_{PGC}. UAV data were collected on September 24 and October 16, and ground data were collected on September 25 and October 21 in 2020. Letter a,b, and c above bars indicate different statistical groups ($\alpha = 0.05$, Duncan test).

approaches. The combined 10-class unsupervised classifications performed better than 2-class unsupervised classifications. However, the end-user will need to determine how to combine the 10-classes into binary classification while using the 10-classification.

3.5. Vegetation indices with thresholds

NDVI with a threshold of 0.3 achieved R^2 of 0.91–0.95 for seashore paspalum and 0.83–0.94 for zoysiagrass, performing the best among all VI_{threshold} methods. These R^2 values were reduced to 0.89–0.90 and

0.78–0.86 for NDRE with a threshold of 0.2. The VARI with a threshold of 0 has an R^2 of 0.64–0.70 and 0.42–0.57 for seashore paspalum and zoysiagrass, respectively. The multispectral bands derived VIs, especially NDVI, with threshold approaches had good overall performance. However, it did not show a good consistency from time to time, especially for zoysiagrass. The R^2 is 0.94 and 0.83 for first-round and second-round, respectively. In addition, the threshold value needs to be determined empirically, which also introduces users' bias. Furthermore, the proper threshold estimations will likely vary between different species, sensors, and sites, making comparisons relatively difficult.

3.6. Machine learning based on vegetation indices

The NDVI_k-means has R^2 of 0.89–0.92 for seashore paspalum and 0.79–0.91 for zoysiagrass, and the NDRE_k-means has an R^2 of 0.62–0.87 for seashore paspalum and 0.40–0.74 for zoysiagrass. The NDVI_k-means showed an acceptable overall performance, and it is relatively easy to use where the user only needs to apply 2-class k-means classification to NDVI data. However, like the NDVI_threshold, NDVI_k-means is not consistent sometimes. The R^2 value of zoysiagrass was reduced from 0.91 of first-round of data to 0.79 of second-round of data because the performance really depends on separability of each dataset. Besides, the mean absolute error is as high as 13.93%, which indicates this approach may be suitable for comparing the relative PGC but may not be suitable for accurately estimating the absolute PGC values.

3.7. RGB image processing approaches

The introduced GPI method achieved R^2 of 0.94–0.96 for seashore paspalum and 0.86–0.93 for zoysiagrass, while Canopeo achieved 0.89–0.95 and 0.80–0.91, respectively. Although Canopeo exhibits high correlations in estimating green cover, the introduced GPI method showed the lowest absolute errors (1.82–2.50%) among all methods compared. However, it is important to recognize that the GPI is based on a similar principle as used in digital image analysis, resulting in observed higher levels of correlation.

In summary, the methods with average R^2 higher than 0.80 showed substantial potential for calculating UAV_{PGC}. Among these compared methods, the GPI and SVM classification based on different band composites demonstrated low error and high correlation as compared to ground data. Considering RGB sensors usually less expensive than multispectral sensors, GPI and RGB-based SVM methods were found to offer a practical solution to calculate turfgrass green cover. The six-band composite did not appear to offer any advantage over the three bands CIR multispectral composite in turfgrass fields. From the complexity aspect, the GPI method, which requires several empirical parameters, is easier to use as compared to the SVM classification, which needs a data training procedure. NDVI_k-means is also an option to calculate turfgrass green cover due to its relative ease of use. However, the user will need to compromise the potential large absolute errors. Even though the GPI method balances high correlation with ground data, low absolute error, ease of use, and low cost, this study provides information to users to select proper methods based on their budget and objectives. We also found that NIR-based methods have the potential to be used for coverage estimation instead of green cover estimation since NIR is sensitive to vegetation no matter it is green or not.

4. Conclusion

This study demonstrated the application of UAV-based remote sensing in determining plot green cover in turfgrasses during the establishment period. A total of thirty methods for UAV_{PGC} estimation were compared and evaluated based on their level of complexity and their correlation coefficient and error rates with the conventional standard ground_{PGC} methods. The introduced GPI method achieved R^2 ranging from 0.86 to 0.96, with MAE ranging from 1.82 to 2.50%. The

GPI method only requires an input of hue and saturation values of greenness using RGB images and therefore, offers ease of use in practice. The SVM classification based on RGB composites is another good option with R^2 ranging from 0.88 to 0.95, with MAE ranging from 1.94 to 2.97%. SVM classification provides good correlation and consistency but requires a well-trained dataset, which may not be a viable option for those with a limited machine learning experience. Nevertheless, the results of GPI and RGB_SVM ($R^2 = 0.86–0.96$) reveal that the RGB sensor could be suitable for estimating the percent green cover of turfgrasses during the establishment period. Overall, the low complexity methods are easy to use for the users who do not have too much experience of remote sensing, while the moderate and high complexity methods could have higher accuracy on green cover estimation. High complexity methods are more suitable for users who have the substantial knowledge of remote sensing.

CRediT authorship contribution statement

Tianyi Wang: Conceptualization, Methodology, Software, Data curation, Writing – original draft, Writing – review & editing, Visualization, Investigation, Validation. **Ambika Chandra:** Conceptualization, Methodology, Writing – review & editing, Resources, Supervision, Project administration, Funding acquisition. **Jinha Jung:** Conceptualization, Writing – review & editing, Methodology. **Anjin Chang:** Writing – review & editing, Methodology.

Declaration of Competing Interest

The authors declare that they have no known competing financial interests or personal relationships that could have appeared to influence the work reported in this paper.

Acknowledgments

This research was funded by Texas A&M AgriLife Research, USDA National Institute of Food and Agriculture (NIFA), Hatch Project TEXO-1-9264 (accession 1003983) and USDA-NIFA funded SCRI project # 2019-51181-30472. The authors thank Meghyn Meeke for operating SigmaScan software; Justin F. Eads and Siew Teck Kong for the field management of the study site. Authors would also like to acknowledge Turfgrass Water Conservation Alliance (TWCA) for their donation of the light box to the turfgrass breeding program.

Appendix A. Supplementary material

Supplementary data to this article can be found online at <https://doi.org/10.1016/j.compag.2022.106721>.

References

- Abràmoff, M.D., Magalhães, P.J., Ram, S.J., 2004. Image processing with imageJ. *Biophotonics Int.* 11, 36–42. <https://doi.org/10.1201/9781420005615.ax4>.
- Adamsen, F.J., Pinter, P.J., Barnes, E.M., LaMorte, R.L., Wall, G.W., Leavitt, S.W., Kimball, B.A., 1999. Measuring wheat senescence with a digital camera. *Crop Sci.* 39 (3), 719–724. <https://doi.org/10.2135/cropsci1999.0011183X003900030019x>.
- Ashapure, A., Jung, J., Yeom, J., Chang, A., Maeda, M., Maeda, A., Landivar, J., 2019. A novel framework to detect conventional tillage and no-tillage cropping system effect on cotton growth and development using multi-temporal UAS data. *ISPRS J. Photogramm. Remote Sens.* 152, 49–64. <https://doi.org/10.1016/j.isprsjprs.2019.04.003>.
- Ashapure, A., Jung, J., Chang, A., Oh, S., Yeom, J., Maeda, M., Maeda, A., Dube, N., Landivar, J., Hague, S., Smith, W., Texas, A., Korea, S., 2020. Developing a machine learning based cotton yield estimation framework using multi-temporal UAS data. *ISPRS J. Photogramm. Remote Sens.* 169, 180–194. <https://doi.org/10.1016/j.isprsjprs.2020.09.015>.
- Bach, M., Poloschek, C.M., 2006. Optical illusions. *Adv. Clin. Neurosci. Rehabil.* 6, 20–21. <https://doi.org/10.1037/h0072139>.

- Bégué, A., Arvor, D., Bellon, B., Betbeder, J., de Abelleira, D., Ferraz, R.P.D., Lebourgeois, V., Lelong, C., Simões, M., Verón, S.R., 2018. Remote sensing and cropping practices: a review. *Remote Sens.* 10, 1–33. <https://doi.org/10.3390/rs10010099>.
- Bhandari, M., Ibrahim, A.M.H., Xue, Q., Jung, J., Chang, A., Rudd, J.C., Maeda, M., Rajan, N., Neely, H., Landivar, J., 2020. Assessing winter wheat foliage disease severity using aerial imagery acquired from small Unmanned Aerial Vehicle (UAV). *Comput. Electron. Agric.* 176, 105665. <https://doi.org/10.1016/j.compag.2020.105665>.
- Bremer, D.J., Lee, H., Su, K., Keeley, S.J., 2011. Relationships between normalized difference vegetation index and visual quality in cool-season turfgrass: II. Factors affecting NDVI and its component reflectances. *Crop Sci.* 51 (5), 2219–2227. <https://doi.org/10.2135/cropsci2010.12.0729>.
- Brosnan, J.T., Chandra, A., Gaussoin, R.E., Kowalewski, A., Leinauer, B., Rossi, F.S., Soldat, D.J., Stier, J.C., Unruh, J.B., 2020. A justification for continued management of turfgrass during economic contraction. *Agric. Environ. Lett.* 5, 1–8. <https://doi.org/10.1002/ael2.20033>.
- Campos, I., González-Gómez, L., Villodre, J., Calera, M., Campoy, J., Jiménez, N., Plaza, C., Sánchez-Prieto, S., Calera, A., 2019. Mapping within-field variability in wheat yield and biomass using remote sensing vegetation indices. *Precis. Agric.* 20 (2), 214–236. <https://doi.org/10.1007/s11119-018-9596-z>.
- Caturegli, L., Corniglia, M., Gaetani, M., Grossi, N., Magni, S., Migliazzi, M., Angelini, L., Mazzoncin, M., Silvestri, N., Fontanelli, M., Raffaelli, M., Peruzzi, A., Volterrani, M., Hu, X., 2016. Unmanned aerial vehicle to estimate nitrogen status of turfgrasses. *PLoS ONE* 11 (6), e0158268. <https://doi.org/10.1371/journal.pone.0158268>.
- Caturegli, L., Gaetani, M., Volterrani, M., Magni, S., Minelli, A., Baldi, A., Brandani, G., Mancini, M., Lenzi, A., Orlandini, S., Lulli, F., de Bertoldi, C., Dubbini, M., Grossi, N., 2020. Normalized difference vegetation index versus dark green colour index to estimate nitrogen status on bermudagrass hybrid and tall fescue. *Int. J. Remote Sens.* 41 (2), 455–470. <https://doi.org/10.1080/01431161.2019.1641762>.
- Chang, A., Jung, J., Maeda, M.M., Landivar, J., 2017. Crop height monitoring with digital imagery from Unmanned Aerial System (UAS). *Comput. Electron. Agric.* 141, 232–237. <https://doi.org/10.1016/j.compag.2017.07.008>.
- Chang, A., Yeom, J., Jung, J., Landivar, J., 2020. Comparison of canopy shape and vegetation indices of citrus trees derived from UAV multispectral images for characterization of citrus greening disease. *Remote Sens.* 12 (24), 4122. <https://doi.org/10.3390/rs12244122>.
- Chang, A., Jung, J., Yeom, J., Maeda, M.M., Landivar, J.A., Enciso, J.M., Avila, C.A., Anciso, J.R., Wang, J., 2021. Unmanned aircraft system- (UAS-) based high-throughput phenotyping (HTP) for tomato yield estimation. *J. Sens.* 2021, 1–14.
- de Donato, P., Barres, O., Sausse, J., Taquet, N., 2016. Advances in 3-D infrared remote sensing gas monitoring. Application to an urban atmospheric environment. *Remote Sens. Environ.* 175, 301–309. <https://doi.org/10.1016/j.rse.2015.12.045>.
- Duan, B., Fang, S., Zhu, R., Wu, X., Wang, S., Gong, Y., Peng, Y., 2019. Remote estimation of rice yield with unmanned aerial vehicle (uav) data and spectral mixture analysis. *Front. Plant Sci.* 10, 1–14. <https://doi.org/10.3389/fpls.2019.00204>.
- Emmons, R., Rossi, F., 2015. *Turfgrass Science and Management*, fifth ed. Cengage Learning.
- Fauvel, M., Benediktsson, Jón.A., Chanussot, J., Sveinsson, J.R., 2008. Spectral and spatial classification of hyperspectral data using SVMs and morphological profiles. *IEEE Trans. Geosci. Remote Sens.* 46 (11), 3804–3814. <https://doi.org/10.1109/TGRS.2008.922034>.
- Gogoi, N.K., Deka, B., Bora, L.C., 2018. Remote sensing and its use in detection and monitoring plant diseases: a review. *Agric. Rev.* 39, 307–313. <https://doi.org/10.18805/ag.r-1835>.
- Gong, P., Howarth, P.J., 1992. Land-use classification of SPOT HRV data using a cover-frequency method. *Int. J. Remote Sens.* 13 (8), 1459–1471. <https://doi.org/10.1080/01431169208904202>.
- Herrmann, I., Bdolach, E., Montekyo, Y., Rachmilevitch, S., Townsend, P.A., Karnieli, A., 2020. Assessment of maize yield and phenology by drone-mounted superspectral camera. *Precis. Agric.* 21 (1), 51–76. <https://doi.org/10.1007/s11119-019-09659-5>.
- Hong, M., Bremer, D.J., Merwe, D., 2019a. Thermal imaging detects early drought stress in turfgrass utilizing small unmanned aircraft systems. *Agrosyst. Geosci. Environ.* 2 (1), 1–9. <https://doi.org/10.2134/age2019.04.0028>.
- Hong, M., Bremer, D.J., van der Merwe, D., 2019b. Using small unmanned aircraft systems for early detection of drought stress in turfgrass. *Crop Sci.* 59 (6), 2829–2844. <https://doi.org/10.2135/cropsci2019.04.0212>.
- Horst, G.L., Engelke, M.C., Meyers, W., 1984. Assessment of visual evaluation techniques 1. *Agron. J.* 76 (4), 619–622. <https://doi.org/10.2134/agronj1984.00021962007600040027x>.
- Huang, Y., Thomson, S.J., Brand, H.J., Reddy, K.N., 2016. Development and evaluation of low-altitude remote sensing systems for crop production management. *Int. J. Agric. Biol. Eng.* 9, 1–11. <https://doi.org/10.3965/j.ijabe.20160904.2010>.
- Huang, B., Zhao, B., Song, Y., 2018. Urban land-use mapping using a deep convolutional neural network with high spatial resolution multispectral remote sensing imagery. *Remote Sens. Environ.* 214, 73–86. <https://doi.org/10.1016/j.rse.2018.04.050>.
- Karcher, D.E., Richardson, M.D., 2015. Digital image analysis in turfgrass research, in: *Turfgrass: Biology, Use, and Management*, pp. 1133–1149. doi: 10.2134/agronmonogr56.c29.
- Karcher, D.E., Richardson, M.D., 2005. Batch analysis of digital images to evaluate turfgrass characteristics. *Crop Sci.* 45 (4), 1536–1539. <https://doi.org/10.2135/cropsci2004.0562>.
- Kranjic, N., Medak, D., Zupan, R., Rezo, M., 2019. Machine learning methods for classification of the green infrastructure in city areas. *IOP Conf. Ser. Earth Environ. Sci.* 362 (1), 012079. <https://doi.org/10.1088/1755-1315/362/1/012079>.
- Krans, J.V., Morris, K., 2007. Determining a profile of protocols and standards used in the visual field assessment of turfgrasses: a survey of national turfgrass evaluation program-sponsored university scientists. *Appl. Turfgrass Sci.* 4 (1), 1–6.
- Lu, D., Weng, Q., 2007. A survey of image classification methods and techniques for improving classification performance. *Int. J. Remote Sens.* 28 (5), 823–870. <https://doi.org/10.1080/01431160600746456>.
- Maimaitjiang, M., Sagan, V., Sidike, P., Hartling, S., Esposito, F., Fritschi, F.B., 2020. Soybean yield prediction from UAV using multimodal data fusion and deep learning. *Remote Sens. Environ.* 237, 111599. <https://doi.org/10.1016/j.rse.2019.111599>.
- Morris, K.N., Shearman, R.C., 1998. NTEP Turfgrass Evaluation Guidelines. NTEP turfgrass evaluation workshop, Beltsville, MD.
- Mountrakis, G., Im, J., Ogole, C., 2011. Support vector machines in remote sensing: a review. *ISPRS J. Photogramm. Remote Sens.* 66 (3), 247–259. <https://doi.org/10.1016/j.isprsjprs.2010.11.001>.
- Oh, S., Chang, A., Ashpore, A., Jung, J., Dube, N., Maeda, M., Gonzalez, D., Landivar, J., 2020. Plant counting of cotton from UAS imagery using deep learning-based object detection framework. *Remote Sens.* 12 (18), 2981. <https://doi.org/10.3390/rs12182981>.
- Pal, M., Mather, P.M., 2005. Support vector machines for classification in remote sensing. *Int. J. Remote Sens.* 26 (5), 1007–1011. <https://doi.org/10.1080/01431160512331314083>.
- Patrignani, A., Ochsner, T.E., 2015. Canopeo: a powerful new tool for measuring fractional green canopy cover. *Agron. J.* 107 (6), 2312–2320. <https://doi.org/10.2134/agronj15.0150>.
- Przeszlowska, A., Trlica, M.J., Weltz, M.A., 2006. Near-ground remote sensing of green area index on the shortgrass prairie. *Rangel. Ecol. Manag.* 59 (4), 422–430. <https://doi.org/10.2111/05-059R1.1>.
- Richardson, M.D., Karcher, D.E., Purcell, L.C., 2001. Quantifying turfgrass cover using digital image analysis. *Crop Sci.* 41 (6), 1884–1888. <https://doi.org/10.2135/cropsci2001.1884>.
- Romero, M., Luo, Y., Su, B., Fuentes, S., 2018. Vineyard water status estimation using multispectral imagery from an UAV platform and machine learning algorithms for irrigation scheduling management. *Comput. Electron. Agric.* 147, 109–117. <https://doi.org/10.1016/j.compag.2018.02.013>.
- Samseemoung, G., Soni, P., Jayasuriya, H.P.W., Salokhe, V.M., 2012. Application of low altitude remote sensing (LARS) platform for monitoring crop growth and weed infestation in a soybean plantation. *Precis. Agric.* 13 (6), 611–627. <https://doi.org/10.1007/s11119-012-9271-8>.
- Smith, A.R., 1978. Color gamut transform pairs. *Comput. Graph. (ACM)* 12 (3), 12–19.
- Su, J., Liu, C., Coombes, M., Hu, X., Wang, C., Xu, X., Li, Q., Guo, L., Chen, W., 2018. Wheat yellow rust monitoring by learning from multispectral UAV aerial imagery. *Comput. Electron. Agric.* 155, 157–166. <https://doi.org/10.1016/j.compag.2018.10.017>.
- Trenholm, L.E., Carrow, R.N., Duncan, R.R., 1999. Relationship of multispectral radiometry data to qualitative data in turfgrass research. *Crop Sci.* 39 (3), 763–769. <https://doi.org/10.2135/cropsci1999.0011183X003900030025x>.
- Tucker, C.J., Miller, L.D., Pearson, R.L., 1975. Shortgrass prairie spectral measurements. *Photogramm. Eng. Remote Sensing* 41, 1157–1162.
- Wang, T., Thomasson, J.A., Isakeit, T., Yang, C., Nichols, R.L., 2020a. A Plant-by-plant method to identify and treat cotton root rot based on UAV remote sensing. *Remote Sens.* 12, 2453. <https://doi.org/10.3390/rs12152453>.
- Wang, T., Thomasson, J.A., Yang, C., Isakeit, T., Nichols, R.L., 2020b. Automatic classification of cotton root rot disease based on UAV remote sensing. *Remote Sens.* 12, 1310. <https://doi.org/10.3390/rs12081310>.
- Wang, T., Thomasson, J.A., Yang, C., Isakeit, T., Nichols, R.L., Collett, R.M., Han, X., Bagnall, C., 2020c. Unmanned aerial vehicle remote sensing to delineate cotton root rot. *J. Appl. Remote Sens.* 14, 034522. <https://doi.org/10.1117/1.JRS.14.034522>.
- Yang, C., Westbrook, J.K., Suh, C.P.C., Martin, D.E., Hoffmann, W.C., Lan, Y., Fritz, B.K., Goolsby, J.A., 2014. An airborne multispectral imaging system based on two consumer-grade cameras for agricultural remote sensing. *Remote Sens.* 6, 5257–5278. <https://doi.org/10.3390/rs6065257>.
- Yang, C., Odvody, G.N., Fernandez, C.J., Landivar, J.A., Minzenmayer, R.R., Nichols, R.L., 2015a. Evaluating unsupervised and supervised image classification methods for mapping cotton root rot. *Precis. Agric.* 16 (2), 201–215. <https://doi.org/10.1007/s11119-014-9370-9>.
- Yang, W., Wang, S., Zhao, X., Zhang, J., Feng, J., 2015b. Greenness identification based on HSV decision tree. *Inf. Process. Agric.* 2 (3–4), 149–160. <https://doi.org/10.1016/j.inpa.2015.07.003>.
- Zhang, J., Virk, S., Porter, W., Kenworthy, K., Sullivan, D., Schwartz, B., 2019. Applications of unmanned aerial vehicle based imagery in turfgrass field trials. *Front. Plant Sci.* 10, 1–12. <https://doi.org/10.3389/fpls.2019.00279>.